Scripta Materialia 205 (2021) 114185

Contents lists available at ScienceDirect

Scripta Materialia

journal homepage: www.elsevier.com/locate/scriptamat

Multilayer co-fired microwave dielectric ceramics in $MgTiO_3$-Li_2TiO_3 system with linear temperature coefficient of resonant frequency

Tao Yue[a,b], Lingxia Li[a,b,*], Mingkun Du[a,b,*], Yu Zhan[a,b]

[a] School of Microelectronics, Tianjin University, Tianjin 300072, China
[b] Institute of Electronic Materials and Components, Tianjin University, Tianjin 300072, China

ARTICLE INFO

Article history:
Received 6 April 2021
Revised 23 July 2021
Accepted 2 August 2021
Available online 16 August 2021

Keywords:
Electronic ceramics
Composites
Scanning electron microscopy
Finite element analysis
Wide temperature stability

ABSTRACT

To address the nonlinear variation of resonant frequency in a $MgTiO_3$-$CaTiO_3$ system over a wide temperature range (-40–105°C), $MgTiO_3$-Li_2TiO_3 system ceramics with multilayer architectures are designed. Trilayer $MgTiO_3$-Li_2TiO_3-$MgTiO_3$ ceramics (mass ratio=0.2:0.56:0.2) sintered at 1275°C possess a linear and near-zero temperature coefficient of resonant frequency (τ_{f+}=-3.0 ppm/°C (25–105°C), τ_{f-}=2.7 ppm/°C (-40–25°C)). Compared with that of random distribution-type $MgTiO_3$-Li_2TiO_3 ceramics, the $Q \times f$ value of trilayer ceramics is significantly improved ($Q \times f$=80,000 GHz (@7.6 GHz)). The electric field distribution is examined by the eigenmode solver of High Frequency Structure Simulator software to analyze the effect of the Li_2TiO_3 content and the stacking scheme on the dielectric properties. The cross-sectional morphologies show a dense intermediate layer formed by ion diffusion, which acts as a glue to bond each layer. This work can be conceived as a new strategy for developing 5G wireless communication components with linear temperature-related resonant frequency (-40–105°C) and low dielectric loss.

The global climate is complicated. Winter temperatures can drop to -40°C in some high-latitude regions, while summer temperatures can be higher than 45°C in some African regions, driving a higher demand for temperature-stable communication equipment [1,2]. Microwave dielectric ceramics (MWDCs), the cornerstone of fifth-generation communication technology (5G), are regarded as critical for communication systems to meet this requirement. However, studies on the temperature stability of the resonant frequency of MWDCs have mostly focused on the positive temperature range, whereas the negative temperature range has been largely neglected.

$MgTiO_3$ ceramic systems, which have outstanding microwave dielectric properties, suitable densities, abundant raw materials and low prices (ε_r=17, $Q \times f$=160,000 GHz (@7 GHz) and ρ<3.6 g/cm^3), can basically meet the needs of 5G devices, except for the τ_f value that deviates from zero (τ_f=-50 ppm/°C) [3–5]. Recently, the two-phase composite method was used in $0.95MgTiO_3$-$0.05CaTiO_3$ system ceramics, achieving a near-zero τ_f value (20–80°C) [6,7]. Unfortunately, little attention has been directed toward negative-temperature range stability. In our study, the nonlinear resonant frequency of a $0.93MgTiO_3$-$0.07CaTiO_3$ ceramic (MT-CT) varied with temperature, leading to suboptimal temperature stability over a wide temperature range. When the positive τ_f value (25–105°C) was tuned to zero, the negative τ_f value (-40–25°C) was approximately +20 ppm/°C mainly due to the temperature dependence of the dielectric constant of the $CaTiO_3$ system.

Recently, Zhou et al. achieved remarkable strides in low-temperature fired Li_2TiO_3 ceramics, and found that the dielectric constant of the Li_2TiO_3 system changes smoothly with temperature, which is essentially different from the $CaTiO_3$ system [8–10]. To improve the linearity of the resonant frequency of the $MgTiO_3$ system, Li_2TiO_3 is selected as the additive and better temperature stability is achieved with $MgTiO_3$-Li_2TiO_3 system ceramics. Traditional randomly distributed processes inevitably lead to varied defects due to possible incompatibility between crystal structure, ionic charge and ionic radius. To reduce defects and possible chemical reactions, multilayer ceramics are proposed. Generally, dielectric properties are related to the Li_2TiO_3 content and the stacking scheme. With the aid of a High Frequency Structure Simulator from Ansoft Company (ANSOFT HFSS), we investigated the electric field distribution of different stacking schemes and found that the middle layer played a significant role in overall performance. This multilayer ceramic with linear temperature coefficient of resonant frequency over a wide temperature range and a high $Q \times f$ value can be envisioned as a pioneering material for 5G.

$MgTiO_3$, Li_2TiO_3 and $CaTiO_3$ (MT, LT, and CT, respectively) powders were separately synthesized by the conventional solid-state

* Corresponding authors at: School of Microelectronics, Tianjin University, Tianjin 300072, China.
E-mail addresses: Li_ling_xia_tju@163.com (L. Li), dmkun@tju.edu.cn (M. Du).

https://doi.org/10.1016/j.scriptamat.2021.114185
1359-6462/

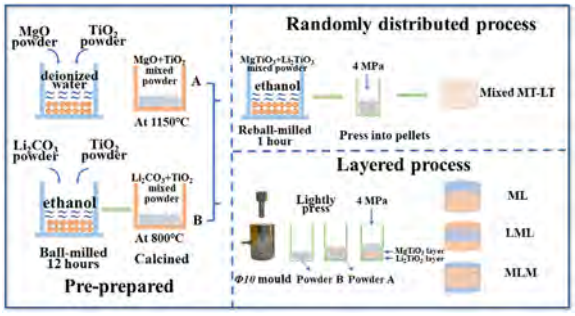

Fig. 1. Schematic diagram of randomly distributed and layered process.

method with high-purity MgO (98%), Li_2CO_3 (98%) and TiO_2 (99%) powders. The powders were weighted according to the desired stoichiometry by a one over ten thousand analytical balance (AW120; Shimadzu Corporation). To achieve an excellent matching characteristic in the diameter direction after co-firing at 1275°C, $MgTiO_3$ and Li_2TiO_3 powders were calcined at 1150°C and 800°C for 4 h in air, respectively. In addition, $CaTiO_3$ powders were calcined at 1100°C for 4 h in air.

Fig. 1 shows a graphical representation of the randomly distributed and layered processes for $MgTiO_3$-Li_2TiO_3 system ceramics. $MgTiO_3$-Li_2TiO_3-$MgTiO_3$ (MLM), Li_2TiO_3-$MgTiO_3$-Li_2TiO_3 (LML) and $MgTiO_3$-Li_2TiO_3 (ML) ceramics with multilayer architectures were prepared by a layered process. The calcinated $MgTiO_3$ and Li_2TiO_3 powders were ground with 8 wt% paraffin as a binder. Based on the composition of $0.4gMgTiO_3$-$xgLi_2TiO_3$ (x=0.5, 0.52, 0.54, 0.56, 0.58), the two powders were alternately added to the mold in three kinds of order. Random distribution-type $MgTiO_3$-Li_2TiO_3 (mixed MT-LT) was synthesized by a randomly distributed process. The calcined $MgTiO_3$ and Li_2TiO_3 powders were mixed according to the mass fraction and then remilled in alcohol for 1 h. In addition, the $0.93MgTiO_3$-$0.07CaTiO_3$ ceramic was also prepared by a randomly distributed process for comparison. The calcined $MgTiO_3$ and $CaTiO_3$ powders were mixed according to the mole ratio and then remilled in deionized water for 1 h. After being dried, the two kinds of mixed powders were ground with 8 wt% paraffin as a binder. All the samples were pressed into pellets with dimensions of 10 mm in diameter and 4–5 mm in thickness under a pressure of 4 MPa for 60 s and then sintered at 1275°C for 4 h in air. The heating rate of the samples was 5 °C/min.

The X-ray diffraction (XRD) patterns of the as-prepared samples were recorded using an X-ray powder diffractometer (D/MAX-2500; Rigaku, Tokyo, Japan) in the range of $10° \leq 2\theta \leq 80°$ using Cu-Kα radiation. Scanning electron microscopy (SEM) and energy dispersive spectrometry (EDS) were used for microstructure observation and cross-sectional analysis (FE-SEM, S-4800; Hitachi, Ltd., Tokyo, Japan). The microwave dielectric performance was measured in TE_{011} mode with a network analyzer (8720ES; Agilent) according to Hakki-Coleman's method and modified by Courtney. The unload Q value was measured by the cavity method. The test system for τ_f values consists of a dielectric resonator (QWED company) and a wide temperature cabinet (GZ-ESPEC GMC-71). The resonant frequencies were obtained by holding the system for 30 min at -40°C, 25°C and 105°C, and the τ_f values were calculated using Eq. (1) and (2):

$$\tau_{f+} = \frac{f_{105} - f_{25}}{f_{25}(T_{105} - T_{25})} \times 10^6 (\text{ppm}/^\circ\text{C}) \quad (1)$$

$$\tau_{f-} = \frac{f_{-40} - f_{25}}{f_{25}(T_{-40} - T_{25})} \times 10^6 (\text{ppm}/^\circ\text{C}) \quad (2)$$

As shown in Fig. 2a, the XRD patterns of the calcined and sintered $MgTiO_3$ powders show similar peaks that can be indexed to the pure $MgTiO_3$ phase (JCPDS #06-0494). The detectable reflection peaks of calcined Li_2TiO_3 powders are indexed to the rock-salt monoclinic phase of pure Li_2TiO_3 (JCPDS #33-0831). After the calcined Li_2TiO_3 powders were sintered at 1275°C for 4 h, the intensity of the (002) peak increased while the intensity of the (-133) peak decreased, indicating an increase in the degree of order and better crystallinity [11]. Fig. 2b shows the XRD patterns of the trilayer MLM ceramics with different mass ratios. To confirm the mass ratio of these two phases, the Rietveld refinement method is adopted, and the calculated pattern fits well with the measured pattern as shown in Fig. 2c–g. Fig. 2h shows that the variation trend is similar to the experimental results, but the test values of the Li_2TiO_3 volume fraction are slightly lower, which may be due to the phenomenon of a solid solution between $MgTiO_3$ and Li_2TiO_3 [12].

Polished and thermal-etched cross-sectional micrographs of the trilayer $MgTiO_3$-Li_2TiO_3-$MgTiO_3$ ceramic architecture were investigated by SEM and EDS. Fig. 3a shows a schematic view of the trilayer MLM ceramic, and Fig. 3b shows an SEM image of the corresponding position. The distribution of element and phase composition was analyzed by EDS (see Table. 1). According to the EDS analysis results, spots A and H are Li_2TiO_3 and $MgTiO_3$. The left side of the SEM image pertains to the Li_2TiO_3 layer, while the right side belongs to the $MgTiO_3$ layer. Meanwhile, the diffusion of Mg^{2+} and Li^+ within a certain range generates a dense intermediate layer, which acts as a glue to bond the layers, thus avoiding the aging of

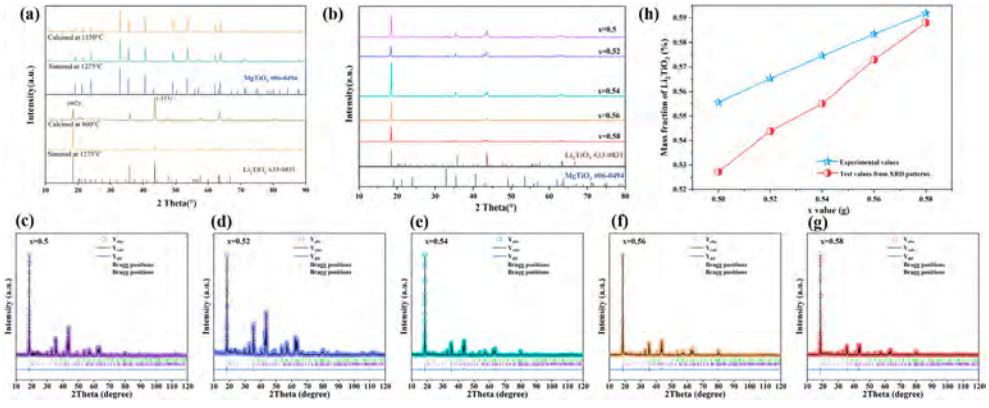

Fig. 2. XRD patterns of as-prepared samples: (a) calcined and sintered $MgTiO_3$ and Li_2TiO_3 powders; (b) trilayer $MgTiO_3$-Li_2TiO_3-$MgTiO_3$ ceramic with different mass ratios; (c)–(g) XRD refinement results; (h) mass fraction of Li_2TiO_3 in the trilayer $MgTiO_3$-Li_2TiO_3-$MgTiO_3$ ceramic.

Table 1
EDS data of selected spots marked in the SEM image in Fig. 3.

Spot	Mg (at.%)	Ti (at.%)	O (at.%)	Spot	Mg (at.%)	Ti (at.%)	O (at.%)
A	4.21	25.00	70.78	E	12.97	26.04	61.00
B	2.66	29.63	67.71	F	11.21	31.07	57.72
C	4.29	23.60	72.11	G	12.66	26.16	61.18
D	3.89	25.79	70.32	H	17.64	23.90	58.46

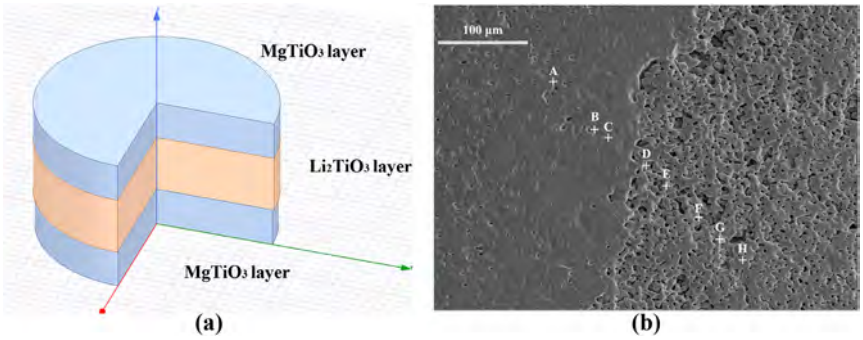

Fig. 3. Lengthwise SEM micrographs for MLM ceramic.

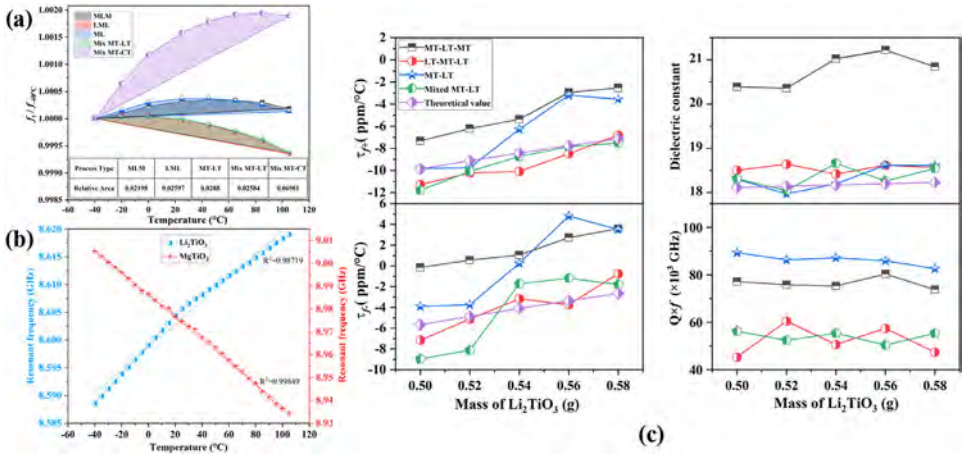

Fig. 4. Variation of (a) *R* values and (b) resonant frequency with temperature. (c) Microwave dielectric properties of $MgTiO_3$-Li_2TiO_3 system ceramics.

traditional organic glue during operation and compensating for the tiny difference in diameter between the two materials.

To illustrate the linear variation of resonant frequency with temperature, the resonant frequencies at multiple temperatures were measured, and the relative resonant frequencies were calculated using the following equation:

$$R = \frac{f_t}{f_{-40^\circ C}} \tag{3}$$

where f_t is the resonant frequency at each temperature point. Fig. 4a presents the *R* values of the $MgTiO_3$-Li_2TiO_3 system ceramic (mass ratio=0.4:0.56) and the random distribution-type $0.93MgTiO_3$-$0.07CaTiO_3$. The *R* values of MT-CT exhibit a relatively flat, horizontal curve section in the positive temperature range (25–105°C), indicating a near-zero τ_f value, but a steep curve section in the negative temperature range (-40–25°C). Similar nonlinear variations of f_0 with temperature and the temperature dependence of τ_f are manifested in the Al_2O_3-TiO_2 system ceramic. Li et al. suggested that these values are determined by the dielectric mixing rules (as shown in Eq. (4)) [13].

$$\tau_{f,C} = \frac{1}{V_1\varepsilon_{r,1}^{\alpha} + V_2\varepsilon_{r,2}^{\alpha}}\left[V_1\varepsilon_{r,1}^{\alpha}\left(\tau_{f,1} + \alpha_{L,1}\right) + V_2\varepsilon_{r,2}^{\alpha}\left(\tau_{f,2} + \alpha_{L,2}\right)\right] - \alpha_{L,C} \quad (-1 \le \alpha \le 1) \tag{4}$$

where the subscripts C, 1 and 2 indicate the composite, Al_2O_3 and TiO_2 phases, respectively, V is the volume fraction, ε_r is the dielectric constant, τ_f is the temperature coefficient of the resonant frequency, α_L is the linear thermal expansion coefficient, and the α value is a determinable value related to the mixing process. From Eq. (4), one can conclude that the temperature-dependent τ_f and ε_r are the main factors affecting the $\tau_{f,C}$ value. Due to the large variation in the dielectric constant of $CaTiO_3$ with temperature, the τ_f value of the $0.93MgTiO_3$-$0.07CaTiO_3$ ceramic is not a constant [14,15]. In turn, the resonant frequency shows nonlinear variation with temperature.

Compared with that of $CaTiO_3$, the dielectric constant of Li_2TiO_3 changes more slowly with temperature, and the influence of dielectric constant changes on τ_f is weakened [9,10]. Furthermore, the dielectric constant of Li_2TiO_3 (~19.8) is close to that of $MgTiO_3$ (~17.0), which is essentially different from the dielectric constant of $CaTiO_3$ (~170.0). For $MgTiO_3$-Li_2TiO_3 system ceramics, ε_{MgTiO_3} and $\varepsilon_{Li_2TiO_3}$ are approximately equal. Therefore, Eq. (4) can be rewritten as follows:

$$\tau_{f,C} = \frac{1}{V_{MgTiO_3} + V_{Li_2TiO_3}}\begin{bmatrix} V_{MgTiO_3}\left(\tau_{f,MgTiO_3} + \alpha_{L,MgTiO_3}\right) \\ +V_{Li_2TiO_3}\left(\tau_{f,Li_2TiO_3} + \alpha_{L,Li_2TiO_3}\right)\end{bmatrix} - \alpha_{L,C} \tag{5}$$

According to Eq. (5), the linear thermal expansion coefficient of the composite ($\alpha_{L,C}$) is assumed to change linearly with the

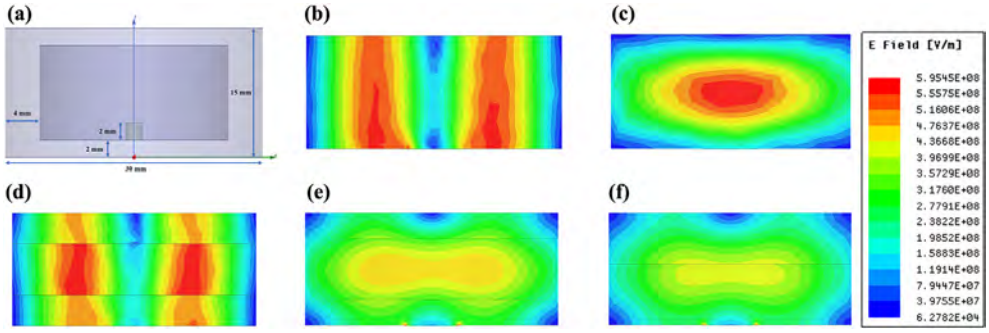

Fig. 5. (a) Diagrammatic drawing of the simulation model and simulation results using the HFSS eigenmode solver in different stacking schemes: (b) $MgTiO_3$, (c) Li_2TiO_3, (d) LML, (e) MLM, and (f) ML (mass ratio of $MgTiO_3$ and Li_2TiO_3 = 0.4:0.56).

mass fraction of Li_2TiO_3; thus, the $\tau_{f,C}$ value is mainly determined by $\tau_{f,MgTiO_3}$ and τ_{f,Li_2TiO_3}. Fig. 4b shows that the resonant frequency changes linearly with the temperature of Li_2TiO_3 and $MgTiO_3$ (R-squared to the straight line is 0.98719 and 0.99849, respectively), which indicates the relative stability of $\tau_{f,MgTiO_3}$ and τ_{f,Li_2TiO_3}. Thus, the relative frequency curves of the $MgTiO_3$-Li_2TiO_3 system are practically flattened in the entire temperature range (-40–105°C). Among the several multilayer ceramics with different stacking schemes, the curves are slightly different. We calculated the relative area of the polygon formed by the curve and the baseline (shown in Fig. 4a). Conceivably, the relative area should approach zero when the curve shows satisfactory linearity. The relative areas are in the order of MLM<mixed MT-LT<LML<ML, which indicates better linearity in the MLM ceramics.

The microwave dielectric properties of multilayer ceramics with different stacking schemes and Li_2TiO_3 contents were measured and compared with randomly distributed samples sintered at 1275°C (see Fig. 4b). Simultaneously, the theoretical values of the randomly distributed samples were also given for comparison. The τ_f values of $MgTiO_3$ and Li_2TiO_3 are -56.3/21.5 ppm/°C in the positive temperature range and -56.6/28.8 ppm/°C in the negative temperature range, respectively. Assuming that $MgTiO_3$ and Li_2TiO_3 can coexist with each other, the theoretical values (τ_f, ε_r) are calculated according to the following empirical formula:

$$ln\varepsilon_r = V_1 ln\varepsilon_{r1} + V_2 ln\varepsilon_{r2} \quad (6)$$

$$\tau_f = V_1\tau_{f1} + V_2\tau_{f2} \quad (7)$$

where V_1 and V_2, ε_{r1} and ε_{r2}, and τ_{f1} and τ_{f2} are the volume percentages, dielectric constants and temperature coefficients of the resonant frequency of the $MgTiO_3$ and Li_2TiO_3 phases respectively [10,16]. Compared with the theoretical values, the measured results of mixed MT-LT have similar trends but with slight deviations, which may be due to the difficulty of forming pure two-phase composite ceramics using the conventional mixed route.

In marked contrast, the multilayer ceramics show more positive τ_f values and better Q × f values. Compared with that of the mixed MT-LT (mass ratio=0.4:0.56), the Q × f value of trilayer MLM ceramic is significantly improved by approximately 60%. The multilayer architecture could effectively restrict the chemical reaction between $MgTiO_3$ and Li_2TiO_3 and reduce the influence of defects and second phases on the dielectric properties, resulting in certain differences between the random distribution-type and multilayer ceramics.

By comparison, the dielectric properties of multilayer ceramics with different stacking schemes have similar variation trends. However, different stacking schemes show large variations in τ_f values, Q × f values and dielectric constants. For example, with 0.56 g Li_2TiO_3, the MLM ceramic shows ε_r~21.2, Q × f~80,000 GHz (@7.6 GHz), τ_{f+}~-3.0 ppm/°C, and τ_{f-}~+2.7 ppm/°C, while the LML ceramic shows ε_r~18.6, Q × f~57,000 GHz (@7.7 GHz), τ_{f+}~-8.5 ppm/°C, and τ_{f-}~-3.7 ppm/°C, and the ML ceramic shows ε_r~18.6, Q × f~86,000 GHz (@7.9 GHz), τ_{f+}~-3.2 ppm/°C, τ_{f-}~4.8 ppm/°C. Notably, the amount of Li_2TiO_3 required in these multilayer ceramics to achieve a near-zero τ_f is in the order of MLM < ML < mixed MT-LT < LML, indicating that the multilayer architecture plays a certain role in regulating the temperature coefficient and can substantially affect the microwave dielectric properties. To further explore the above differences, the eigenmode solver was used to examine the electric field distributions for different stacking schemes by ANSOFT HFSS.

The finite element method was used to simulate the electric field distribution of the intrinsic resonance of dielectric resonators. Fig. 5a displays a diagrammatic drawing of the simulation model whose size is based on actual values in the experiment. Fig. 5b and Fig. 5c show the electric field distribution of $MgTiO_3$ and Li_2TiO_3 ceramic resonators, respectively. The heights of $MgTiO_3$ (3.7727 mm) and Li_2TiO_3 (4.1703 mm) ceramics are fairly close. Excluding the effect of size on simulations, $MgTiO_3$ and Li_2TiO_3 ceramics showed distinctive electric field distributions. Understandably, the

Table 2
Microwave dielectric properties of typical MgO-TiO_2 and Li_2O-TiO_2 system materials.

Material system	Materials	Q × f (GHz)	ε_r	τ_f (ppm/°C)	Temperature range	Ref.
MgO-TiO_2 system	(1-x)$Mg_{(1.04-3/2y)}Ce_yTiO_3$-x$CaTiO_3$	71,000	23.0	0.0	20–80°C	[22]
	(1-x)$Mg_{0.95}Ni_{0.05}Ti_{0.98}Zr_{0.02}O_3$ -x$Ca_{0.6}La_{0.8/3}TiO_3$	116,000	23.9	-2.0	20–80°C	[23]
	0.92$MgTiO_3$-0.08$NaTaO_3$	55,000	19.4	+1.1	30–90°C	[24]
	(1-x)$MgTiO_3$-x($Ca_{0.6}Na_{0.2}Sm_{0.2}$)TiO_3	76,000	22.8	-3.1	25–85°C	[25]
	$MgTiO_3$-5wt%CaF_2	37,000	17.5	4.8	25–80°C	[26]
Li_2TiO_3 system	(1-x)Li_2TiO_3-xLi_2CeO_3	59,000	21.2	-7.4	20–80°C	[27]
	0.3Li_2TiO_3-0.7Li($Zn_{0.5}Ti_{1.5}$)O_4	88,000	23.5	-0.8	25–85°C	[28]
	Li_2TiO_3-20vol.%$Li_2Zn_3Ti_4O_{12}$	28,000	22.0	-1.6	25–75°C	[29]
	0.7Li_2TiO_3-0.3ZnO	100,000	23.0	0.0	25–80°C	[11]
	MLM (mass ratio=0.2:0.56:0.2)	80,000	21.2	-3.0/2.7	**-40–105°C**	This work

electric field distributions of different stacking schemes were noticeably different. Fig. 5d–f presents the electric field distributions of multilayer ceramics with different stacking schemes (mass ratio of $MgTiO_3$:Li_2TiO_3=0.4:0.56). In contrast with that of the LML ceramic, the electric field of the ML ceramic tends to concentrate at the bottom due to its asymmetric structure. Li_2TiO_3 shows a positive τ_f value (τ_{f+}=21.5, τ_{f-}=28.8) with a higher ε_r than $MgTiO_3$ [16–19]. Some studies have indicated that the distribution of the electric field is affected by the distribution of the dielectric constant and is relatively concentrated in the layer with a high dielectric constant, suggesting that the Li_2TiO_3 layer has a denser electric field distribution in the ML structure [16,20,21]. Moreover, since the dielectric constants of $MgTiO_3$ and Li_2TiO_3 are similar, the electric field distribution of the trilayer architecture is heavily influenced by the middle layer, which plays a more important role in overall performance. Accordingly, one may speculate that the order for the amount of Li_2TiO_3 required to achieve a near-zero τ_f is MLM < ML < LML.

The microwave dielectric properties of typical MgO-TiO_2 system and Li_2O-TiO_2 system materials are summarized in Table 2. The current trilayer MLM ceramic clearly has excellent dielectric properties. In addition, the wide-temperature stability of MgO-TiO_2 system materials was studied and reported for the first time. With the advantage of wide-temperature stability and excellent microwave dielectric properties, the results of this study can be applied to the development of 5G wireless communication components.

In this paper, we selected $MgTiO_3$ as the matrix, and $MgTiO_3$-Li_2TiO_3 system ceramics with random distribution-type and multilayer architectures were prepared. With a mass ratio of $MgTiO_3$:Li_2TiO_3=0.4:0.56, the trilayer $MgTiO_3$-Li_2TiO_3-$MgTiO_3$ ceramic has excellent properties: ε_r=21.2, Q × f=80,000 GHz (@7.6 GHz) and τ_{f+}=-3.0 ppm/°C, τ_{f-}=2.7 ppm/°C. In contrast to the random distribution-type $MgTiO_3$-Li_2TiO_3, the Q × f value is significantly improved by approximately 60%. This design provides a stable operation scheme over a wide temperature range (-40–105°C).

Declaration of Competing Interest

None.

Acknowledgments

This work was supported by the National Key R&D Program of China [Grant No. 2017YFB0406300].

References

[1] L.Z. Ni, L.X. Li, M.K. Du, J. Alloy. Compd. 844 (2020) 156106.
[2] L.Z. Ni, L.X. Li, M.K. Du, Y. Zhan, Ceram. Int. 47 (2021) 1034–1039.
[3] N. Santha, M. Rakhi, G. Subodh, Mater. Chem. Phys. 255 (2020) 123636.
[4] C.L. Huang, J.L. Hou, C.L. Pan, C.Y. Huang, C.W. Peng, C.H. Wei, Y.H. Huang, J. Alloy. Compd. 450 (2008) 359–363.
[5] Z.P. Xu, L.X. Li, S.H. Yu, M.K. Du, W.J. Luo, J. Alloy. Compd. 802 (2019) 1–5.
[6] Y.B. Chen, J. Alloy. Compd. 478 (2009) 657–660.
[7] H. Li, B. Tang, X. Li, Z.J. Qing, Y.X. Li, H. Yang, Q. Wang, S.R. Zhang, J. Mater. Sci. 49 (2014) 5850–5855.
[8] H.H. Guo, D. Zhou, L.X. Pang, J.Z. Su, J. Mater. 4 (2018) 368–382.
[9] H.H. Guo, M.S. Fu, D. Zhou, C. Du, P.J. Wang, L.X. Pang, W.F. Liu, A.S.B. Sombra, J.Z. Su, ACS Appl. Mater. Interfaces 13 (2021) 912–923.
[10] H.H. Guo, D. Zhou, C. Du, P.J. Wang, W.F. Liu, L.X. Pang, Q.P. Wang, J.Z. Su, C. Singh, S. Trukhanov, J. Mater. Chem. C 8 (2020) 4690–4700.
[11] C.L. Huang, Y.W. Tseng, J.Y. Chen, J. Eur. Ceram. Soc. 32 (2012) 3287–3295.
[12] W.J. Luo, L.X. Li, B.W. Zhang, J.L. Qiao, J. Alloy. Compd. 824 (2020) 153978.
[13] L. Li, S. Yang, S.Y. Wu, X.M. Chen, Appl. Phys. Lett. 118 (21) (2021) 212902.
[14] H.Y. Zhou, X.Q. Liu, X.L. Zhu, X.M. Chen, J. Am. Ceram. Soc. 101 (5) (2018) 1999–2008.
[15] V.V. Lemanov, A.V. Sotnikov, E.P. Smirnova, M. Weihnacht, R. Kunze, Solid State Commun. 110 (11) (1999) 611–614.
[16] J. Zhang, Z.X. Yue, Y. Luo, L.T. Li, Ceram. Int. 44 (2018) 21000–21003.
[17] H.Z. Zuo, X.L. Tang, H. Guo, Q.G. Wang, C.L. Dai, H.W. Zhang, H. Su, Ceram. Int. 43 (16) (2017) 13913–13917.
[18] J.J. Bian, Y.M. Ding, Ceram. Int. 40 (2014) 3595–3601.
[19] Y.Z. Hao, H. Yang, G.H. Chen, Q.L. Zhang, J. Alloy. Compd. 552 (2013) 173–179.
[20] J. Zhang, Y. Luo, Z.X. Yue, L.T. Li, J. Am. Ceram. Soc. 102 (2019) 342–350.
[21] S. Wang, W.J. Luo, L.X. Li, M.K. Du, J.L. Qiao, J. Eur. Ceram. Soc. 41 (2021) 418–423.
[22] W. Gong, B. Ullah, W. Lei, G.F. Fan, X.H. Wang, W.Z. Lu, Ceram. Int. 43 (2017) 3051–3056.
[23] A. Manan, Z. Ullah, A.S. Ahmad, A. Ullah, D.F. Khan, A. Hussain, M.U. Khan, J. Adv. Ceram. 7 (2018) 72–78.
[24] K.G. Wang, H.F. Zhou, X.W. Luan, S. Hu, X.J. Zhou, S. He, X. Wang, S.C. Zhou, X.L. Chen, Ceram. Int. 47 (2021) 121–129.
[25] L.X. Li, S. Li, T. Tian, X.S. Lyu, J. Ye, H. Sun, J. Mater. Sci. Mater. Electron. 27 (2016) 1286–1292.
[26] J. Zhang, Z.X. Yue, X.H. Zhang, L.T. Li, Ceram. Int. 41 (2015) S515–S519.
[27] W.Q. Liu, R.Z. Zuo, J. Eur. Ceram. Soc. 38 (2018) 119–123.
[28] Y. Wu, D. Zhou, J. Guo, L.X. Pang, H. Wang, X. Yao, Mater. Lett. 65 (2011) 2680–2682.
[29] A. Sayyadi-Shahraki, E. Taheri-Nassaj, S.A. Hassanzadeh-Tabrizi, H. Barzegar-Bafrooei, J. Alloy. Compd. 597 (2014) 161–166.